Tight-binding energy dispersions of armchair-edge graphene nanostrips

D. Gunlycke and C. T. White
Naval Research Laboratory, Washington, D.C. 20375, USA
(Received 30 January 2008; published 12 March 2008)

A tight-binding model of hydrogen-terminated armchair-edge graphene nanostrips is presented, which includes up to third-nearest-neighbor carbon-carbon interactions and edge distortion. The model reproduces the band gaps found in first-principles local-density-functional calculations well. The model also leads to energy dispersion relations in excellent agreement with first-principles results in the vicinity of the Fermi level. Approximate analytical $\vec{k}\cdot\vec{p}$ and effective mass expressions of the dispersion relations are also presented. Finally, the electron-phonon coupling constant is estimated to be 40 eV/nm.

DOI: 10.1103/PhysRevB.77.115116 PACS number(s): 73.22.Dj, 73.61.Wp, 73.63.Fg

I. INTRODUCTION

The observation of a single stable sheet of graphite,[1] known as graphene, has suggested a new candidate material for the next generation of electronic devices. Unlike other materials supporting conventional two-dimensional electronic gases, graphene has dispersion relations that feature a strong linear behavior in the energy region near the Fermi level.[2] This linear behavior near the Fermi level is also found in the one-dimensional dispersion relations of metallic single-wall carbon nanotubes,[3,4] in spite of the curvature and lateral confinement of these tubes. As a one-dimensional material with excellent electrical properties,[5,6] nanotubes are suitable for a range of nanoscale applications.[7] Because of their close kinship to single-wall carbon nanotubes, this might also be true for narrow strips of graphene,[8] which are normally referred to as graphene nanostrips or graphene nanoribbons.

There are different types of graphene nanostrips.[9] The two main ones, with the edges assumed terminated by hydrogen atoms, are often referred to as armchair-edge and zigzag-edge nanostrips, because of the arrangements of carbon atoms along the nanostrip edges. Zigzag-edge nanostrips exhibit edge-localized states[10,11] and are believed to spin polarize spontaneously.[12,13] Armchair-edge nanostrips, however, have no edge-localized states[11] and do not spin polarize. The electronic structure of armchair-edge nanostrips is closely related to that of zigzag nanotubes,[14] and both materials exhibit a one-electron band gap with a period three modulation in the confined in-plane direction.[11]

Some models have predicted that one-third of the armchair-edge nanostrips are metallic.[11,15–17] However, another model found that distortion converts these metallic nanostrips into semiconductors.[18] More recently, it was discovered that there are one-electron band gaps in all armchair-edge nanostrips even without distortion, due to third-nearest-neighbor carbon-carbon interactions.[14] The existence of band gaps in all armchair-edge nanostrips has been confirmed by independent first-principles local-density-functional (LDF) calculations.[12,14,19] Whereas the band gaps in those nanostrips first predicted to be metallic have been attributed to either lattice distortion[12,18] or neglect of third-nearest-neighbor carbon-carbon interactions,[14] it is shown herein that both effects must be included to arrive at tight-binding band structures in good agreement with corresponding first-principles LDF results in the presence of edge distortions.

The first-principles LDF band structure data presented in this paper are obtained by using an approach that includes all electrons and forms linear combinations of atomic orbitals.[20,21] The orbitals are approximated using uncontracted Gaussian orbitals, $7s3p$ for carbon atoms and $3s$ for hydrogen atoms.[22] All carbon-carbon (carbon-hydrogen) bond lengths are taken as 0.142 (0.111) nm, except for those carbon-carbon bonds connecting carbon atoms that are also bonded to hydrogen atoms. Relaxation calculations[12] have shown that the latter bonds are about 3.5% shorter than other carbon-carbon bonds in the strip. Therefore, these bond lengths have been determined to be 0.137 nm, which is also consistent with an earlier study including distortion.[18] The LDF band structure data reported are collected from calculations by using 64 evenly spaced k points in the first Brillouin zone.

II. TIGHT-BINDING MODEL

An armchair-edge graphene nanostrip can be recognized by the armchair-like pattern that the outermost carbon atoms form along the edges of a narrow strip of graphene. Across the strip, carbon atoms form zigzag chains. Consider an arbitrary nanostrip with N carbon atoms in each such chain. To compensate for the dangling carbon sp^2 bonds at each chain end, we assume that the nanostrip is terminated with hydrogen atoms. As all σ bonds are filled in the hydrogen-terminated nanostrip, it is sufficient to only consider orthonormal π orbitals, of which there is one per carbon atom. The graphene nanostrip can then be viewed as a graphene sheet with imposed Dirichlet boundary conditions to ensure that the π wave functions of interest vanish at the strip edges (see Fig. 1). These boundary conditions can be used to define an effective width $w=(N+1)a/2$ of the nanostrip, where $a \approx 0.246$ nm is the graphene lattice constant. With this relation in mind, the appearances of $N+1$ throughout the paper can be interpreted in terms of a dimensionless nanostrip width.

A tight-binding Hamiltonian of the armchair-edge nanostrip can be written as a sum of contributions,

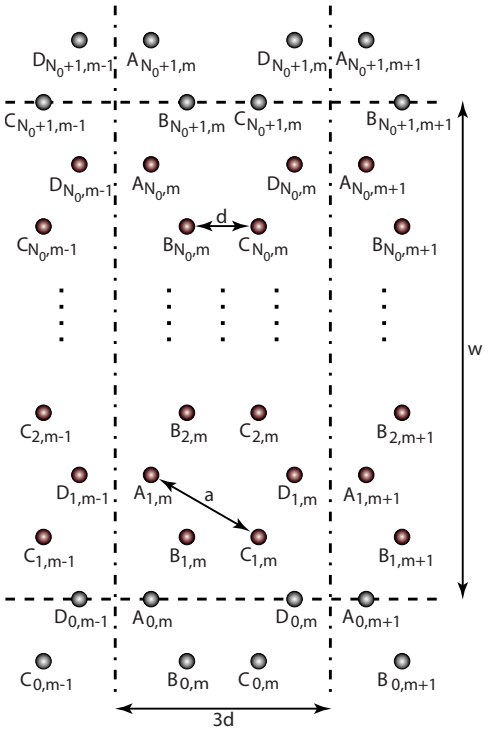

FIG. 1. (Color online) Labeled carbon atoms in a graphene honeycomb lattice. Consider all atoms entirely between the two dashed lines to be a part of a staggered N armchair-edge graphene nanostrip extending horizontally. The nanostrip is divided into translational unit cells divided by the dash-dotted lines. In each unit cell, there are four types of carbon atoms, labeled A–D, which are repeated vertically $N_0 \equiv N/2$ times.

$$\hat{H} = \hat{H}_1 + \hat{H}_3 + \hat{H}_{3t} + \hat{H}_{1d}, \tag{1}$$

where $\hat{H}_1$ represents the usual first-nearest-neighbor (1NN) Hamiltonian,[2] $\hat{H}_3$ represents a third-nearest-neighbor (3NN) Hamiltonian,[14] $\hat{H}_{3t}$ is a 3NN truncation term, and $\hat{H}_{1d}$ is a 1NN edge distortion term.[12] The 3NN truncation term is a correction to the 3NN term (more details are provided below). Note that second-nearest-neighbor (2NN) interactions are not included in the model, because, to a good approximation, they merely rigidly shift the dispersion relations in the region of interest near the Fermi level.[14] Likewise, small changes in the on-site carbon matrix elements due to the presence of the hydrogen atoms at the strip edges are neglected as these perturbations, again to a good approximation, rigidly shift the dispersion relations in the region of interest.[14]

By using electron creation and annihilation operators, $c^{\tau\dagger}_{n,m}$ and $c^{\tau}_{n,m}$, respectively, which act on the π state associated with the site labeled $\tau_{n,m}$ in Fig. 1, the terms in Eq. (1) can be expressed, assuming N even,[23] as follows:

$$\hat{H}_1 = \gamma_1 \sum_{n,m} [(c^{B\dagger}_{n,m} + c^{B\dagger}_{n+1,m} + c^{D\dagger}_{n,m-1})c^{A}_{n,m} + (c^{D\dagger}_{n-1,m} + c^{D\dagger}_{n,m} + c^{B\dagger}_{n,m})c^{C}_{n,m} + \text{H.c.}], \tag{2a}$$

$$\hat{H}_3 = \gamma_3 \sum_{n,m} [(c^{D\dagger}_{n-1,m-1} + c^{D\dagger}_{n+1,m-1} + c^{D\dagger}_{n,m})c^{A}_{n,m} + (c^{B\dagger}_{n-1,m} + c^{B\dagger}_{n+1,m} + c^{B\dagger}_{n,m+1})c^{C}_{n,m} + \text{H.c.}], \tag{2b}$$

$$\hat{H}_{3t} = -\gamma_3 \sum_{m} [c^{B\dagger}_{0,m}c^{C}_{1,m} + c^{D\dagger}_{N_0+1,m-1}c^{A}_{N_0,m} + \text{H.c.}], \tag{2c}$$

$$\hat{H}_{1d} = \Delta\gamma_1 \sum_{m} [c^{B\dagger}_{1,m}c^{C}_{1,m} + c^{D\dagger}_{N_0,m-1}c^{A}_{N_0,m} + \text{H.c.}], \tag{2d}$$

where $\gamma_1 \approx -3.2$ eV and $\gamma_3 \approx -0.3$ eV are 1NN and 3NN hopping parameters,[14] respectively, and $\Delta\gamma_1 \equiv \gamma_1' - \gamma_1$ is a distortion parameter fitted to $\Delta\gamma_1 \approx -0.2$ eV later in the paper. Furthermore, $n = 1, 2, \ldots, N/2$ and $m = 1, 2, \ldots, M$, where $M(\to\infty)$ is the number of translational unit cells. In addition to all hopping terms describing physical connections in the nanostrip, there are terms in Eqs. (2a) and (2b) involving artificial carbon atoms located along the horizontal dashed lines of Fig. 1. However, because of the imposed boundary conditions, the wave functions vanish on these artificial atoms, so that these additional terms have no impact on the calculations. There are, nevertheless, terms in Eq. (2b) describing 3NN interactions across these dashed lines. The purpose of the 3NN truncation Hamiltonian in Eq. (2c) is to exactly cancel these nonphysical cross-boundary terms. Finally, Eq. (2d) describes a distortion of the bonds in the strip direction that is closest to the edges.[12]

To obtain analytical energy dispersion relations, it is useful to transform the Hamiltonian using

$$c^{\tau}_{n,m} = \frac{2}{\sqrt{N+1}} \sum_{p} \sin\frac{(2n - \lambda_\tau)p\pi}{N+1} \bar{c}^{\tau}_{p,m}, \tag{3a}$$

$$\bar{c}^{\tau}_{p,m} = \frac{1}{\sqrt{M}} \sum_{\kappa} e^{-i\kappa m} \bar{c}^{\tau}_{p,\kappa}, \tag{3b}$$

where $\lambda_\tau = 0$ for $\tau \in \{A, D\}$ and $\lambda_\tau = 1$ for $\tau \in \{B, C\}$, $p = 1, 2, \ldots, N/2$ is a band index, and κ $[-\pi \leqslant \kappa < \pi]$ is a dimensionless phase defined in terms of the one-dimensional wave vector k by $\kappa \equiv 3kd$, where $d \approx 0.142$ nm is the carbon-carbon bond length. After some algebra, the Hamiltonian terms in Eq. (2) can be expressed as follows:

$$\hat{H}_1 = \gamma_1 \sum_{p,\kappa} \left[2\cos\frac{p\pi}{N+1} (\bar{c}^{B\dagger}_{p,\kappa}\bar{c}^{A}_{p,\kappa} + \bar{c}^{D\dagger}_{p,\kappa}\bar{c}^{C}_{p,\kappa}) + (e^{-i\kappa}\bar{c}^{D\dagger}_{p,\kappa}\bar{c}^{A}_{p,\kappa} + \bar{c}^{B\dagger}_{p,\kappa}\bar{c}^{C}_{p,\kappa}) + \text{H.c.} \right], \tag{4a}$$

$$\hat{H}_3 = \gamma_3 \sum_{p,\kappa} \left[2\cos\frac{2p\pi}{N+1} (e^{-i\kappa}\bar{c}^{D\dagger}_{p,\kappa}\bar{c}^{A}_{p,\kappa} + \bar{c}^{B\dagger}_{p,\kappa}\bar{c}^{C}_{p,\kappa}) + (\bar{c}^{D\dagger}_{p,\kappa}\bar{c}^{A}_{p,\kappa} + e^{i\kappa}\bar{c}^{B\dagger}_{p,\kappa}\bar{c}^{C}_{p,\kappa}) + \text{H.c.} \right], \tag{4b}$$

$$\hat{H}_{3t} \approx \frac{4\gamma_3}{N+1}\sum_{p,\kappa}\left[\sin^2\frac{p\pi}{N+1}(e^{-i\kappa}\bar{c}^{D\dagger}_{p,\kappa}\bar{c}^{A}_{p,\kappa} + \bar{c}^{B\dagger}_{p,\kappa}\bar{c}^{C}_{p,\kappa}) + \text{H.c.}\right], \tag{4c}$$

$$\hat{H}_{1d} \approx \frac{4\Delta\gamma_1}{N+1}\sum_{p,\kappa}\left[\sin^2\frac{p\pi}{N+1}(e^{-i\kappa}\bar{c}^{D\dagger}_{p,\kappa}\bar{c}^{A}_{p,\kappa} + \bar{c}^{B\dagger}_{p,\kappa}\bar{c}^{C}_{p,\kappa}) + \text{H.c.}\right], \tag{4d}$$

where the small terms coupling different p's have been neglected in Eqs. (4c) and (4d). This approximation results in a Hamiltonian that gives the exact same energy dispersion as that obtained from the original Hamiltonian to first order in γ_3/γ_1 and $\Delta\gamma_1/\gamma_1$.

Another band index $s=\pm 1$ can be introduced corresponding to combinations of the pairs (D,A) and (B,C). Letting

$$\bar{c}^{A}_{p,\kappa} = (v_{1,p,\kappa} + v_{-1,p,\kappa})e^{i\kappa/2}/\sqrt{2},$$

$$\bar{c}^{B}_{p,\kappa} = (u_{1,p,\kappa} - u_{-1,p,\kappa})/\sqrt{2},$$

$$\bar{c}^{C}_{p,\kappa} = (v_{1,p,\kappa} - v_{-1,p,\kappa})/\sqrt{2},$$

$$\bar{c}^{D}_{p,\kappa} = (u_{1,p,\kappa} + u_{-1,p,\kappa})e^{-i\kappa/2}/\sqrt{2} \tag{5}$$

allows the Hamiltonian to be simplified to

$$\hat{H} = \sum_{s,p,\kappa}[z_{s,p,\kappa}u^{\dagger}_{s,p,\kappa}v_{s,p,\kappa} + z^{*}_{s,p,\kappa}v^{\dagger}_{s,p,\kappa}u_{s,p,\kappa}], \tag{6}$$

where

$$z_{s,p,\kappa} = \gamma_1\left(2se^{i\kappa/2}\cos\frac{p\pi}{N+1} + 1\right) + \gamma_3\left(2\cos\frac{2p\pi}{N+1} + e^{i\kappa}\right) + \frac{4(\gamma_3+\Delta\gamma_1)}{N+1}\sin^2\frac{p\pi}{N+1}. \tag{7}$$

In matrix representation, the Hamiltonian in Eq. (6) is block diagonal, where each block is a 2×2 matrix. By diagonalizing every block independently, the tight-binding energy dispersion of the armchair-edge graphene nanostrip can be obtained as follows:

$$\varepsilon^{\pm}_{sp}(\kappa) = \pm|z_{s,p,\kappa}| = \pm\sqrt{E^2_{sp} + A_{sp}\sin^2\frac{\kappa}{4} + B_p\sin^2\frac{\kappa}{2}}, \tag{8}$$

where

$$E_{sp} \equiv \gamma_1\left(2s\cos\frac{p\pi}{N+1} + 1\right) + \gamma_3\left(2\cos\frac{2p\pi}{N+1} + 1\right) + \frac{4(\gamma_3+\Delta\gamma_1)}{N+1}\sin^2\frac{p\pi}{N+1}, \tag{9a}$$

$$A_{sp} \equiv -8\gamma_1 s\cos\frac{p\pi}{N+1}\left[\gamma_1 + \gamma_3\left(2\cos\frac{2p\pi}{N+1} + 1\right) + \frac{4(\gamma_3+\Delta\gamma_1)}{N+1}\sin^2\frac{p\pi}{N+1}\right], \tag{9b}$$

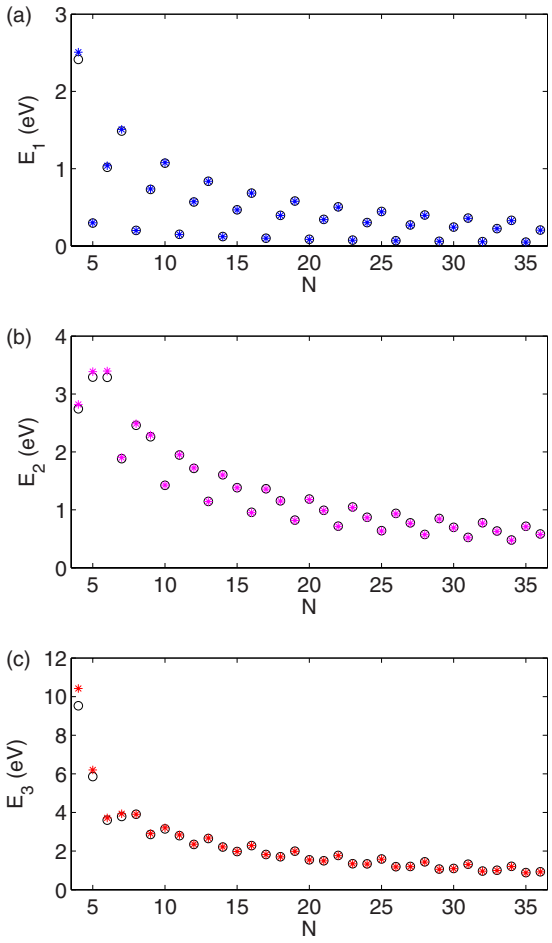

FIG. 2. (Color online) Numerical first-principles and analytical tight-binding zone-center energy separations are compared for armchair-edge graphene nanostrips with various widths without the presence of edge distortion. (a) The energy separation E_1 refers to the zone-center separation between the conduction and valence bands or, simply, the band gap E_g. The first-principles and tight-binding band gaps, shown as circles and stars, respectively, agree well. The agreement also extends to the separations between the second and third conduction-valence-band pair, E_2 and E_3, shown in (b) and (c), respectively.

$$B_p \equiv -4\gamma_3\left(\gamma_1 + 2\gamma_3\cos\frac{2p\pi}{N+1} + \frac{4(\gamma_3+\Delta\gamma_1)}{N+1}\sin^2\frac{p\pi}{N+1}\right). \tag{9c}$$

Because half the nanostrip bands are filled in equilibrium, the tight-binding energy dispersion relations in Eq. (8) exhibit electron-hole symmetry. Equation (8) also shows that the dispersion relations obey time-reversal symmetry. As a consequence of the time-reversal symmetry, the minimum energy separation for corresponding conduction and valence bands near the Fermi level occurs at the zone center and is given by $2|E_{sp}|$.

The minimum separations for the combinations of s and p with the three smallest values of $2|E_{sp}|$ are shown in Figs. 2 and 3 for nanostrips with various widths. Figure 2 shows the energy separations for the case without edge distortion, i.e., $\Delta\gamma_1=0$. These separations are compared to the same separa-

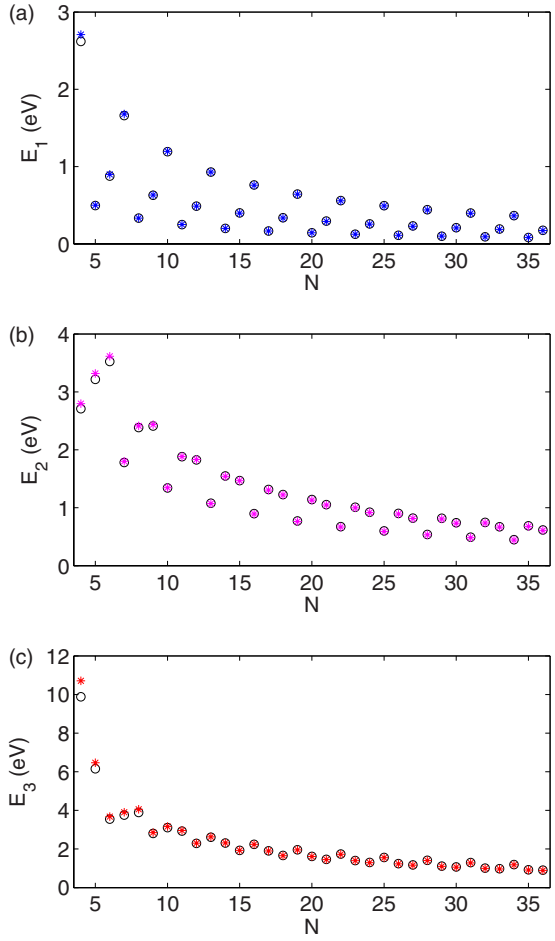

FIG. 3. (Color online) Numerical first-principles and analytical tight-binding zone-center energy separations are compared for armchair-edge edge-distorted graphene nanostrips with various widths. (a)–(c) show the same energy separations as in Fig. 2, but with edge distortion considered in both the first-principles and tight-binding approaches.

tions obtained from the corresponding first-principles calculations. If γ_3 were set to zero, then the tight-binding separations would be zero in Fig. 2(a) for strips with effective widths divisible by 3, which would be in disagreement with the first-principles results. This disagreement, which arises without regard to the magnitude of γ_1, illustrates the importance of including 3NN interactions in the tight-binding model. In Fig. 3, a comparison similar to that made in Fig. 2 is presented, but now in the presence of edge distortion. Note the clearly visible differences between Figs. 2(a) and 3(a), and also between Figs. 2(b) and 3(b). These differences arise from the effects of edge distortion that also must be taken into account in the tight-binding model. To achieve the good quantitative agreement between the tight-binding and first-principles energy separations in Figs. 2 and 3, both 3NN and edge distortion terms must be included.

The smallest and most important energy separation is the band gap. If the dimensionless nanostrip width satisfies $\mathrm{mod}(N+1,3)=0$, then the first set of conduction and valence bands has band indices $s=-1$ and $p=(N+1)/3$. Substituting Eq. (9a) into $E_g=2|E_{-1,(N+1)/3}|$ gives the band gap

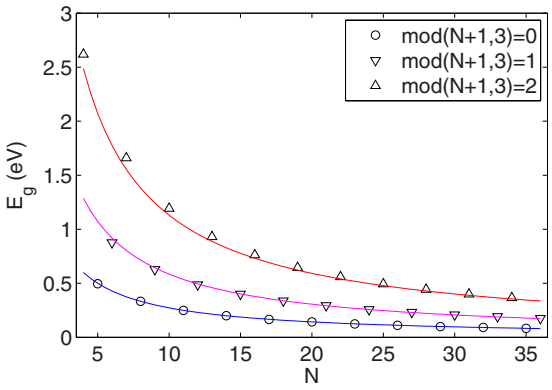

FIG. 4. (Color online) Band gaps for graphene nanostrips with different widths. The open symbols and the solid curves represent first-principles data and analytical expressions given in the text, respectively. There are three types of symbols highlighting a strong modulo dependence of the band gap. Each type has one solid curve associated with it. The solid curve for $\mathrm{mod}(N+1,3)=0$ has been directly fitted to the data using Eq. (10). The curves for $\mathrm{mod}(N+1,3)\neq 0$ follow from an approximate expression [Eq. (11)] assuming large N.

$$E_g = -\frac{6(\gamma_3+\Delta\gamma_1)}{N+1}. \tag{10}$$

From this equation, it is apparent that both 3NN interactions and 1NN distortion contribute to the band gap. It is also from this equation that the distortion parameter, $\Delta\gamma_1\approx -0.2$ eV, was obtained by means of a least-squares fit. Furthermore, if the dimensionless nanostrip width is not a multiple of 3, the lowest conduction and highest valence bands have band indices $s=-1$ and $p=(N+1\mp 1)/3$, where the sign is chosen to make p an integer. The band gaps, for these nanostrips, can then be approximated for large N, which gives

$$E_g \approx -\frac{2\pi(\gamma_1-2\gamma_3)}{\sqrt{3}(N+1)} \pm \frac{6(\gamma_3+\Delta\gamma_1)}{N+1}, \tag{11}$$

where the plus [minus] sign applies to nanostrips satisfying $\mathrm{mod}(N+1,3)=1$ [$\mathrm{mod}(N+1,3)=2$]. The band gap expressions in Eqs. (10) and (11) are compared to the first-principles results in Fig. 4. There is good agreement for the case when $\mathrm{mod}(N+1,3)=0$, as expected from Fig. 3(a) and the fact that Eq. (10) is obtained from Eq. (8) without approximation. However, the agreement is almost as good for the cases where $\mathrm{mod}(N+1,3)\neq 0$, even for narrow nanostrips.

The tight-binding model produces results in good agreement not only with those from first-principles calculations at the zone center, but also for nonzero wave vectors, as can be seen in Fig. 5, which plots the energy dispersions for three nanostrips with different values of $\mathrm{mod}(N+1,3)$. This good agreement between the two methods near the Fermi level suggests that the tight-binding model includes the most important and dominating one-electron effects.

The tight-binding energy dispersion relations in Eq. (8) can be approximated by expanding κ at the zone center, and then substituting $k=\kappa/3d$, to find

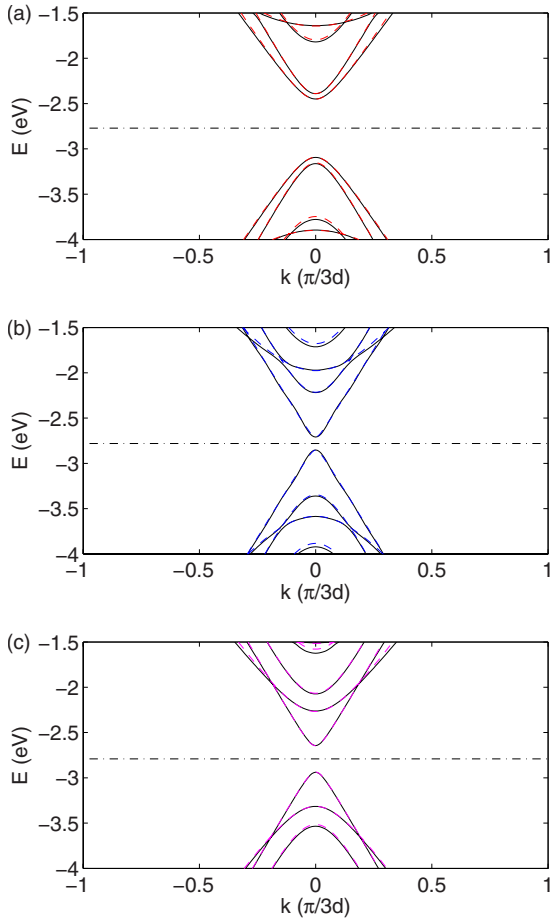

FIG. 5. (Color online) Numerical first-principles and analytical tight-binding energy dispersions, shown as solid and dashed curves, respectively. The dispersions in (a)–(c) are calculated for nanostrips with $N=19$, $N=20$, and $N=21$, in that order. The Fermi levels in the tight-binding calculations have been chosen to be the same as in the corresponding first-principles calculations.

$$\varepsilon_{sp}^{\pm}(k) \approx \pm \sqrt{E_{sp}^2 + (\hbar v_{sp})^2 k^2}, \tag{12}$$

where E_{sp} is defined in Eq. (9a) and

$$\begin{aligned}(\hbar v_{sp})^2 \equiv (3d)^2 \Bigg\{ & -\frac{1}{2}\gamma_1 s \cos\frac{p\pi}{N+1} \\ & \times \Bigg[\gamma_1 + \gamma_3 \left(2\cos\frac{2p\pi}{N+1} + 1 \right) \\ & + \frac{4(\gamma_3 + \Delta\gamma_1)}{N+1} \sin^2\frac{p\pi}{N+1} \Bigg] \\ & - \gamma_3 \Bigg(\gamma_1 + 2\gamma_3 \cos\frac{2p\pi}{N+1} \\ & + \frac{4(\gamma_3 + \Delta\gamma_1)}{N+1} \sin^2\frac{p\pi}{N+1} \Bigg) \Bigg\}. \end{aligned} \tag{13}$$

Note that the same dispersion can also be obtained from $\vec{k}\cdot\vec{p}$ theory by appropriately approximating the momentum matrix elements. By considering the bands with $s=-1$ and $p=(N+1)/3$ in Eq. (13) for nanostrips with $\mathrm{mod}(N+1,3)=0$ in the limit $N\to\infty$, one also finds the Fermi velocity for graphene as follows:

$$v_F = -\frac{3d}{2\hbar}(\gamma_1 - 2\gamma_3), \tag{14}$$

which is consistent with earlier results including the effects of 1NN, 2NN, and 3NN interactions.[14] That this expression is the Fermi velocity for a tight-binding model of graphene including up to 3NN interactions can perhaps be seen most easily by identifying the sublattice coupling within the model, as $\gamma_1 f(\vec{k}) + \gamma_3 f(-2\vec{k})$, where $f(\vec{k}) = \Sigma_i e^{i\vec{k}\cdot\vec{R}_i}$ and $\vec{R}_i$ are the relative locations of the three nearest neighbors of an arbitrary atom. The derivative of this coupling with respect to the magnitude of the wave vector results in the factor $\gamma_1 - 2\gamma_3$ present in the Fermi velocity. With the parameters in this paper, $v_F \approx 8.4\times 10^5$ m/s.

Sometimes it might also be convenient to apply the effective mass approximation. Expanding Eq. (12) to second order in the wave vector simplifies the dispersion relations further to

$$\varepsilon_{hsp}(k) \approx \pm \left[E_{sp} + \frac{\hbar^2 k^2}{2m_{sp}^*} \right], \tag{15}$$

where the effective mass is here defined as $m_{sp}^* \equiv E_{sp}/v_{sp}^2$.

III. CONCLUSIONS

Edge physics plays an important role in the electronic properties of graphene nanostrips. The bands gaps in the armchair-edge nanostrips originally predicted to be metallic arise for at least two reasons: distortion affecting bond lengths at the edges and truncation of 3NN interactions that occurs because of the strip edges. It has been shown that both these effects are necessary to reproduce good tight-binding band structures. From the presented study, one can also estimate the electron-phonon coupling constant as $\alpha \equiv \Delta\gamma_1/\Delta d_1$ where Δd_1 is the change in the carbon-carbon bond length at the edges, as $\alpha \equiv 0.2$ eV/0.005 nm $=40$ eV/nm. This value is slightly smaller than the experimental value $\alpha \approx 45$ eV/nm for graphene.[24] The underestimate of the coupling constant is consistent with another similar estimate from first-principles calculations on all-*trans*-polyacetylene.[21]

Based on the success of the presented one-electron approach, the model should serve as a solid platform for other armchair-edge nanostrip studies involving more complex interactions and/or many-body effects.

ACKNOWLEDGMENTS

D.G. acknowledges support from the Naval Research Laboratory through the National Academies Research Associateship Programs. This work was also supported by the Office of Naval Research through the Naval Research Laboratory. J. W. Mintmire is thanked for discussions.

[1] K. S. Novoselov, A. K. Geim, S. V. Morozov, D. Jiang, Y. Zhang, S. V. Dubonos, I. V. Grigorieva, and A. A. Firsov, Science **306**, 666 (2004).
[2] P. R. Wallace, Phys. Rev. **71**, 622 (1947).
[3] J. W. Mintmire, B. I. Dunlap, and C. T. White, Phys. Rev. Lett. **68**, 631 (1992).
[4] J. W. Mintmire, D. H. Robertson, and C. T. White, J. Phys. Chem. Solids **54**, 1834 (1993).
[5] C. T. White and J. W. Mintmire, J. Phys. Chem. B **109**, 52 (2005).
[6] J.-C. Charlier, X. Blase, and S. Roche, Rev. Mod. Phys. **79**, 677 (2007).
[7] P. Avouris and J. Chen, Mater. Today **9**, 46 (2006).
[8] C. Berger *et al.*, Science **312**, 1191 (2006).
[9] K. Tanaka, S. Yamashita, H. Yamabe, and T. Yamabe, Synth. Met. **17**, 143 (1987).
[10] D. H. Lee and J. D. Joannopoulos, Phys. Rev. B **23**, 4997 (1981).
[11] M. Fujita, K. Wakabayashi, K. Nakada, and K. Kusakabe, J. Phys. Soc. Jpn. **65**, 1920 (1996).
[12] Y.-W. Son, M. L. Cohen, and S. G. Louie, Phys. Rev. Lett. **97**, 216803 (2006).
[13] L. Pisani, J. A. Chan, B. Montanari, and N. M. Harrison, Phys. Rev. B **75**, 064418 (2007).
[14] C. T. White, J. Li, D. Gunlycke, and J. W. Mintmire, Nano Lett. **7**, 825 (2007).
[15] K. Nakada, M. Fujita, G. Dresselhaus, and M. S. Dresselhaus, Phys. Rev. B **54**, 17954 (1996).
[16] M. Ezawa, Phys. Rev. B **73**, 045432 (2006).
[17] L. Brey and H. A. Fertig, Phys. Rev. B **73**, 235411 (2006).
[18] M. Fujita, M. Igami, and K. Nakada, J. Phys. Soc. Jpn. **66**, 1864 (1997).
[19] V. Barone, O. Hod, and G. E. Scuseria, Nano Lett. **6**, 2748 (2006).
[20] J. W. Mintmire and C. T. White, Phys. Rev. Lett. **50**, 101 (1983).
[21] J. W. Mintmire and C. T. White, Phys. Rev. B **28**, 3283 (1983).
[22] F. B. van Duijneveldt, IBM Report No. RJ 945, 1971.
[23] Although leading to minor notational complications, the case when N is odd eventually leads to the same results as in the case where N is even, except for a pair of largely flat bands located away from the Fermi level.
[24] S. Piscanec, M. Lazzeri, J. Robertson, A. C. Ferrari, and F. Mauri, Phys. Rev. B **75**, 035427 (2007).